A Novel Approach to Measuring Separation Process of Oil-Saline Using Differential Electromagnetic Inductive Sensor and FPGA-based Impedance Analyser

DOI:
10.1109/JSEN.2018.2864786

Document Version
Accepted author manuscript

A Novel Approach to Measuring Separation Process of Oil-Saline Using Differential Electromagnetic Inductive Sensor and FPGA-based Impedance Analyser

Shupei Wang*, Ruozhou Hou†, Jorge R. Salas Avila*, Yang Tao*, Wuliang Yin*, *Senior Member, IEEE*

***Abstract*—Liquid-liquid separation is an important process in many chemical engineering applications. The ability to monitoring this process, in particular with a non-contact method is of high value. This paper proposes and implements a novel sensing system adopting a differential electromagnetic inductive sensor (DEMIS) and an FPGA-based (field-programmable gate array) impedance analyser to monitor the separation processes of an oil-in-saline liquid system. The inductive sensor has a concentric cylinder structure with its coils arranged differentially. It is optimised to achieve a homogeneous sensitivity distribution in the sensing region. Electrical models of the oil-saline separation processes are established. Experiments under different oil and saline fractions, different agitation speeds and durations are conducted to validate the capability of the system.**

***Index Terms*—oil-saline separation, differential electromagnetic inductive sensor, sensitivity distribution, liquid-liquid separation model, FPGA.**

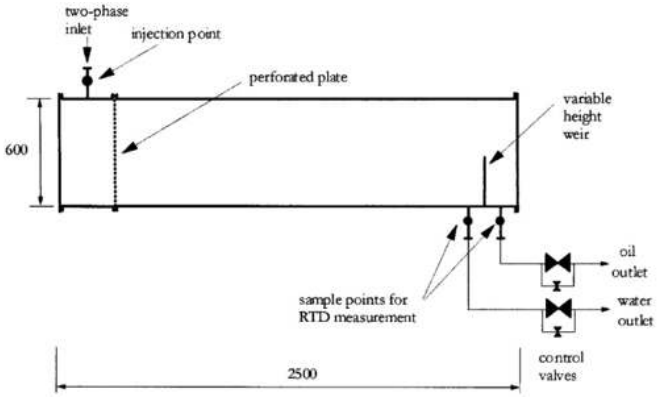

Fig. 1. Schematic diagram of pilot-scale separator and interface positions

I. Introduction

MONITORING the separation process of crude oil extracted from an oil well is of importance in the oil industry. One of the most prevailing separation devices is the American Petroleum Institute (API) oil-saline separator which is illustrated in Fig. 1. At the rear of the API separator, oil flows over the edge of the variable height weir and is recovered through the oil outlet pipe. Saline, on the other hand, is directly disposed of through the outlet pipe connected to the bottom of the primary separation tank. The separation speed of oil and saline is mainly dependent on the oil-saline ratio, and the interface level determines the control strategy of two outlet valve openings which eventually controls the residence time of the oil and saline phases inside the tank [1]. It is therefore essential that the separation process and oil-saline ratio in the separation tank are monitored continuously in order to ensure high production efficiency and product consistency.

Various techniques have been developed for the monitoring of oil-saline separation process. One method involves the use of a sight glass, and the inspection of oil-saline level is conducted by human eyes [2]. However, impurities such as wax and scale in the multiphase flow could coat the wall and obstruct the interface observation through the sight glass.

Shupei Wang, Jorge R. Salas Avila, Yang Tao, Wuliang Yin are with the School of Electrical and Electronic Engineering, and Ruozhou Hou is with the School of Chemical Engineering and Analytical Science, The University of Manchester, Manchester, U.K. The corresponding author is Yang Tao. E-mail: yang.tao@manchester.ac.uk

Another technique takes advantage of mechanical sensors which, for example, employs a level gauge with a sliding displacer of chosen density between oil and saline [3], [4]. The performance of this technique would still tend to be affected by the cleanness of the fluid, as the displacer could be immobilised [5]. Ultrasonic sensors, on the other hand, have the virtue of being contactless and non-invasive. An ultrasonic interface level detector was developed in Norway Christian Michelsen Research (CMR) in 2005 [6]. The proposed ultrasonic sensor was attached to the outside bottom of separator vessel. The detector calculated the vertical distance between the sensor and interface through pulse and echo measurements. However, the accuracy of the sensor may drop significantly due to signal attenuations caused by the presence of air bubbles, foams and emulsions in the system [7].

Vertically segmented sensor probes are also widely adopted in industrial applications. The basic idea of this type of sensors is by combining relevant local information from each individual sensor cell to achieve comprehensive spatial phase distribution information. There are four commonly used sensor types, and they are nucleonic sensors, pressure sensors, capacitance sensors and inductive sensors. The Nucleonic density measurement is considered to be very reliable and accurate in monitoring the interface level of oil-saline separation process [8]. The high performance is achieved by the technique of dual-energy gamma densitometry, which translates the attenuation information corresponding to the absorption coefficient of materials into density profiles [9],

[10]. However, the hazardous nature of gamma radiation leads to extra health and environmental concerns [11]. With respect to pressure sensors, local liquid density profiles are acquired by eliminating liquid height, and gauging pressure components from the output signal [12]. In practical applications, however, the measurement accuracy is likely to degrade when the sensor surface is covered by wax or scale impurities in the flow. Researches on single traversing pressure component driven by a motion system were reported in [13]. One problem of the proposed system was that the wear and tear of motive components would reduce the stability for online monitoring and increase the maintenance cost. In terms of the capacitance sensors, various approaches have been attempted, which include single-electrode probe, separate sensor cells and multiple source electrodes with a common detector [14], etc. Electrical Capacitance Tomography (ECT) in particular was tested by Isaksenet et. al. for interface measurements [15]. The basic principle of ECT is to construct the cross-sectional images of permittivity distribution based on the inter-electrode mutual capacitance measurements of electrode pairs surrounding the process vessel [16], [17]. The main limitation of ECT for the application of oil-saline separation monitoring is that the presence of a conductive phase in the system has a tremendous impact on the quality of the reconstructed images as it would strongly interfere electrical signals acquired by the capacitive electrodes [8]. As another electrical sensing methodology, electromagnetic inductive sensors are widely applied to the level measurement of single phase conductive liquid, e.g. monitoring sea level [18]. A typical inductive sensor system consists of a transmitting coil and a receiving coil. Alternating current is injected into the transmitting coil which generates a primary magnetic field. Eddy currents will be induced within the conductive liquid giving rise to a secondary field which can be detected by the receiving coil. Based upon the induced voltage of the receiving coil, the information of conductivity can be deduced [19]. In order to measure the multiple interface levels that typically exist in a primary oil separator, inductive sensors are distributed evenly along the vertical probe from which sufficient spatial impedance distribution information can be acquired. One example is the Inductive Level Monitoring System (ILMS) developed by the ABB Group [20]. Although the proposed sensor probes were in direct contact with the fluid, impurities hardly had significant effect on the measurement accuracy. However, the saline, if leaking into the wires, would short-circuit the sensor and cause the malfunction of the entire system.

In this paper, we present a non-intrusive and non-invasive differential electromagnetic inductive sensor (DEMIS) and oil-saline separation monitoring system. Sensitivity analysis is carried out in order to give rise to an optimized design of the sensor. An electrical model is proposed, which applies the Maxwell Garnett mixing formula to the oil-saline separation process, and calculates conductivity changes in different separation zones. The proposed model enables the evolution of sensor voltage with respect to separation time under different process conditions to be simulated. Validations of the measurement and sensor systems are subsequently addressed. This is then followed by experimental investigations, in which the performance of the proposed system is assessed under various process conditions including the agitation speed, agitation duration, and oil-saline fraction. Comparing to existing inductive sensing system, there are two main advantages of DEMIS. The first and most important advantage is that DEMIS can be optionally implemented at the outside of a separation vessel so the direct contact with fluids and the potential risk of short-circuit caused by leaking are eliminated. In addition, the relatively larger number of sensors for existing segmented inductive sensor system implies that a more complex data acquisition and processing system is needed, while the DEMIS system requires less. In the remainder of the paper, Section II presents a description of the differential electromagnetic inductive sensor structure, and results from sensitivity analysis, equivalent electrical model calculations and simulation. Section III demonstrates the design of the experimental system. The validation of the system and experimental results are discussed in Section IV. The last section concludes the paper.

II. Model and Simulation

A. Differential Electromagnetic Inductive Sensor

1) Sensor Structure: Comparing to conventional inductive sensors, the differential electromagnetic inductive sensor consists of one cylindrical transmitting coil T and two cylindrical receiving coils R1 and R2 as shown in Fig. 2. The three coils are aligned vertically, with the transmitting coil located in the middle to form two symmetrical testing areas A1 and A2. The transmitting coil is connected to the excitation signal of the impedance analyser. The two receiving coils are connected to form a differential structure. Each coil is wounded five turns with a diameter of 150 mm and the distance between the transmitting coil and each receiving coil is 125 mm. All the coils are wounded on the outside of an empty plastic vessel, so they can be rigidly supported.

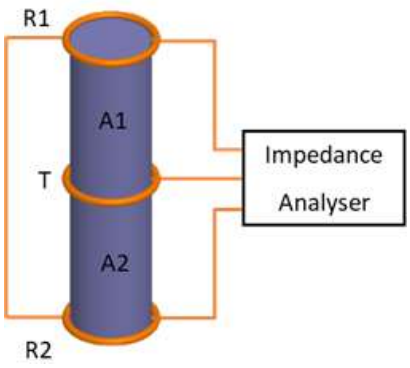

Fig. 2. Schematic of Differential Electromagnetic Inductive Sensor.

2) Sensitivity Analysis: Dyck and Lowther showed that the conductivity sensitivity of a two-coil sensor system can be derived as:

$$S_\sigma = \vec{E_1} \cdot \vec{E_2} \tag{1}$$

where $\vec{E_1}$ and $\vec{E_2}$ are the local electrical field vectors when either of the two coils is excited [21]. Yin and Peyton

This article has been accepted for publication in a future issue of this journal, but has not been fully edited. Content may change prior to final publication. Citation information: DOI 10.1109/JSEN.2018.2864786, IEEE Sensors Journal

considered the motion of a conductive component in the system and its effect on the sensitivity calculations [22]. In the application of this paper, however, this effect is expected to be negligible, since the velocity of the conductive medium in the separation process is small. Using Equation (1) and finite-element method, the axial cross-section sensitivity distribution of a two-coil sensor system was calculated and is shown in Fig. 3. The distance between the two coils was 125 mm while the diameter of both coils was 150 mm. The axial cross-section was divided into 1681 elements.

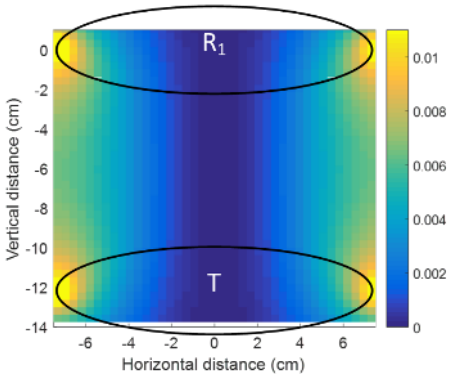

Fig. 3. Axial Cross-section Sensitivity Distribution of 2 Cylindrical Coils.

In order to analyse the spatial sensitivity distribution, the sensitivity values of all the pixels on the same horizontal cross-section are added together to obtain the corresponding planar sensitivity of the horizontal cross-section. The planar sensitivity values represent the sensitivity of each horizontal plane with respect to the conductivity change of homogeneously distributed material on the plane. The cylindrical test region between the two coils in Fig. 3 was divided into 41 individual horizontal planes with corresponding planar sensitivity. The primary task is to reduce the variation of the planar sensitivity. Given a fixed size of sensor coils, the central axial region has more uniform sensitivity than the peripheral region of the coils. However, the absolute sensitivity weaker in the central region. It is therefore important to choose an appropriate vessel size. Planar sensitivity distributions under different radius of the sensing region were calculated and are shown in Fig. 4, in which R stands for the radius of the coils. It is clear that the variation of planar sensitivity distribution reduces with the testing vessel radius, yet the absolute sensitivity value also drops. The average absolute sensitivity values were calculated and are listed in Table I. Since we arbitrarily fixed the size of the coil, and tests showed that the average signal-to-noise ratio (SNR) would be readily above 60 dB when the radius of the test vessel stayed below 50 mm, which met our measurement requirements, we thus decided to choose the diameter of the test vessel to be 100 mm.

TABLE I
AVERAGE ABSOLUTE CROSS-SECTIONAL SENSITIVITY UNDER DIFFERENT TESTING RADIUS.

Testing Radius	1/6 R	2/6 R	3/6 R	4/6 R	5/6 R	R
Average Absolute Sensitivity ($\frac{V^2}{m^2}$)	0.230	0.906	1.991	3.412	5.066	6.706

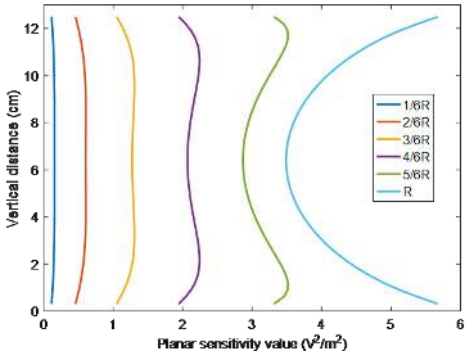

Fig. 4. Planar sensitivity distribution under different testing vessel radius.

B. Electrical Model Of Liquid-Liquid Separation

1) Liquid-liquid Separation Model: A variety of liquid-liquid separation or dispersion models have been proposed from either an experimental or theoretical perspective [23], [24]. For a typical separation process, the liquid volume can be divided into four zones, namely, a clear oil zone, a dense-packed zone, a sedimentation zone and a clear saline zone, as shown in Fig. 5(a). The evolution of the interfaces between the liquid zones can be depicted in Fig. 5(b). In general, oil drops would ascend to form the dense-packed zone and the oil drops at the top of the dense-packed zone would simultaneously coalesce to form the clear oil zone. Therefore, the height of the interface between the clear oil zone and dense-packed zone would decline, while the height of the interface between the sedimentation zone and clear saline zone would increase with time. Since the speed of the sedimentation is faster than that of the coalesce of oil drops, the height of the interface between the dense-packed zone and sedimentation zone decreases until an inflection point t_i when all the oil drops are stacked in the dense-packed zone. After t_i, the height of the dense-packed zone gradually diminishes as oil drops continue to coalesce which gives rise to a clear separation of oil and saline.

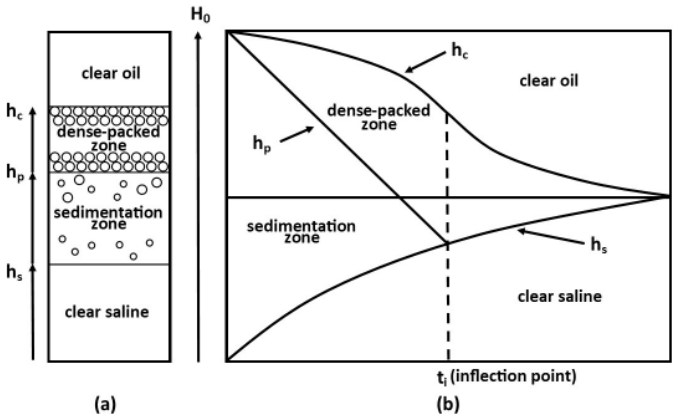

Fig. 5. (a) Four sections defined in oil-saline separation system. (b) Height change of the boundaries of four sections with time.

The functions describing the interface heights was derived in [25] and are expressed in Equation (2), (3), (4), and (5) where h_s denotes the height of the interface between the clear saline

zone and sedimentation zone prior to the inflection point t_i, and h_c denotes the height of the interface between the clear oil zone and dense-packed zone throughout the whole separation process. The height of the interface between the dense-packed zone and sedimentation zone prior and anterior to the inflection point t_i are denoted as h_{p_1} and h_{p_2}, respectively. In the equations H_0 is the initial height of dispersion, while ε_0 and ε_p are the initial oil hold-up fraction and the oil hold-up fraction in the dense-packed zone respectively. The inflection point is represented as t_i. The initial sedimentation velocity of oil drops and the sedimentation velocity of oil drops at the inflection point are denoted as v_0 and v_i respectively. The height h_s at t_i is represented as h_{s_i}. The parameters k_1, k_2, k_3 and k_4 are fitting constants without clear physical meanings and they could be obtained by fitting the equations with practical experiment data.

$$h_s = v_0 t - (v_0 - v_i)\frac{t^2}{t_i} \tag{2}$$

$$h_{p_1} = H_0 - \frac{H_0 - h_{s_i}}{t_i} t \tag{3}$$

$$h_{p_2} = (1-\varepsilon_0)H_0 + (1-\frac{1}{\varepsilon_p})H_0\varepsilon_0(1+k_1 t^{k_2})e^{-k_3 t^{k_4}} \tag{4}$$

$$h_c = (1-\varepsilon_0)H_0 + H_0\varepsilon_0(1+k_1 t^{k_2})e^{-k_3 t^{k_4}} \tag{5}$$

2) Effective Conductivity Model: In order to understand the induced voltage of the receiving coil, an electrical model needs to be derived. Specifically, the effective conductivity of the liquid zones is essential in the calculation of the voltage of receiving coil. The effective conductivity of liquid as a mixture of liquids with two different conductivities σ_1 and σ_2 can be calculated using the Maxwell Garnett mixing formula [26] which is expressed in Equation (6) where σ_{mp} is the effective conductivity and ε is the hold-up fraction of the second liquid drops.

$$\sigma_{mp} = \sigma_1 + 3\varepsilon\sigma_1 \frac{\sigma_2 - \sigma_1}{\sigma_2 + 2\sigma_1 - \varepsilon(\sigma_2 - \sigma_1)} \tag{6}$$

$$\varepsilon_s = \frac{H_0\varepsilon_0 - (H_0 - h_c) - (h_c - h_{p_1})\varepsilon_p}{h_{p_1} - h_s} \tag{7}$$

The oil hold-up fraction in the dense-packed zone ε_p can be considered as constant during the separation process. However, the oil fraction in the sedimentation zone ε_s is changing with time which is expressed as Equation (7) if we assume the oil droplets are evenly distributed. The volumes of the four liquid zones and their evolutions are calculated using Equation (2), (3), (4), and (5). The effective conductivities of each liquid zones can be calculated using Equation (6) and (7). Therefore, the whole electrical model of the separation process are obtained. In practical scenario, the conductivity of crude oil is considered to be zero, and the real time conductivity of saline can be measured through the saline released from saline outlet of the separation vessel, as shown in Fig. 1.

C. Simulation of the electrical liquid-liquid separation model

Before conducting experiments, it is of benefit to study the sensor output by simulation based upon the electrical model in Section II in order to gain a better insight of the separation process. The model relies on additional sensors to acquire the parameters in the interface height functions. For example, a digital CCD camera may be needed to capture the the initial sedimentation velocity of oil drops v_0 and the sedimentation velocity of oil drops at the inflection point v_i. In this section, we adopt the parameters given in [25] and they are listed in Table II. The parameters were evaluated based on practical experiments carried out in a mixing vessel with the diameter of 154 mm and height of 300 mm. With the interface heights and effective conductivity values determined, simulations were carried out for the corresponding separation models and coil sensors in Maxwell®. The simulation geometry is shown in Fig. 6. For the models applied in the simulations, the transmitting coil is excited with a current of 1 A at 1 MHz and the conductivity of saline is 4 S/m.

TABLE II
EXPERIMENTAL PROFILES AND MODEL PARAMETERS ADOPTED FROM [25] FOR H_0=300 MM, D=154 MM, ε_p=0.65 AND ONE-HOUR AGITATION TIME .

Experiment	No. 1	No. 2	No. 3
Agitation speed	350 (RPM)	350 (RPM)	500 (RPM)
ε_0	0.3	0.5	0.5
v_0 (mm/s)	1.1	0.51	0.25
v_i (mm/s)	0.08	0.15	0.06
t_i (s)	153.7	165.0	348.9
h_{s_i} (mm)	91.4	54.9	52.6
k_1 (S^{-k_2})	4.1801×10^{-9}	1.4149×10^{-4}	2.3575×10^{-4}
k_2	3.2264	1.8231	1.4828
k_3 (S^{-k_4})	2.1941×10^{-5}	1.0743×10^{-3}	1.4160×10^{-3}
k_4	1.9770	1.4273	1.1780

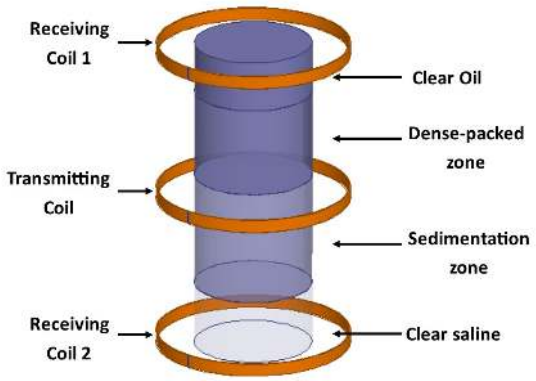

Fig. 6. The model geometry and coil sensors in the simulation.

The real parts of the induced voltages generated during the separation process in both of the receiving coils (V1 and V2) and the differential output are shown in Fig. 7. In this case, we took the second profile in Table II as the input of the simulation. It can be seen that voltage in the upper receiving coil decreases with time. This is because in the upper testing zone, when a separation process starts, the volume of

This article has been accepted for publication in a future issue of this journal, but has not been fully edited. Content may change prior to final publication. Citation information: DOI 10.1109/JSEN.2018.2864786, IEEE Sensors Journal

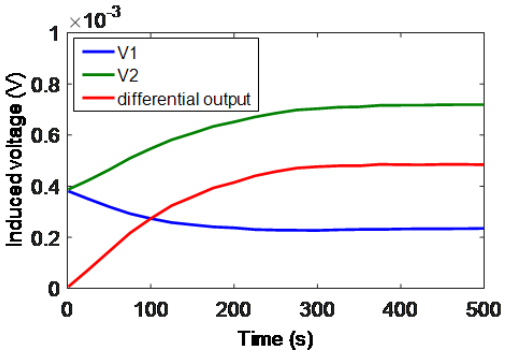

Fig. 7. Induced voltage in both receiving coils and the differential output using profile No. 2 in Table II.

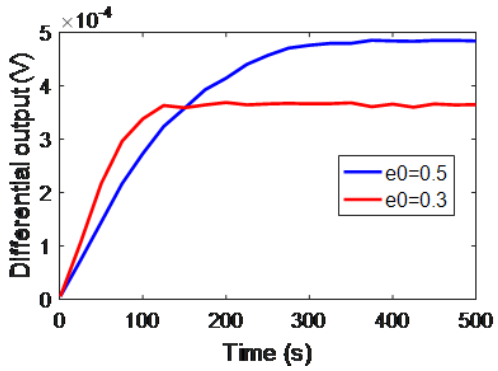

Fig. 9. Sensor outputs of two separation processes using profiles No. 1 and No. 2 in Table II.

saline would gradually decrease while the volume of oil would increase. The increasing voltage in the lower receiving coil can be explained similarly. The overall differential output of the sensor system would increase with time.

For comparison, simulations under different separation speeds were considered. The separation speed of the liquid system is mainly dependent on the buoyance and coalescence of oil droplets. The buoyance velocity of an independent sphere oil droplet in the continuous saline phase can be calculated by the Stokes' law [27] which is expressed as:

$$v = \frac{2}{9}\frac{\rho_w - \rho_o}{\mu} g R^2 \tag{8}$$

where g is gravitational acceleration, ρ_0 and ρ_w are the mass density of oil and saline respectively, μ is the dynamic viscosity of oil and R is the radius of the oil droplet. This equation indicates that the buoyance speed decreases as the oil droplet size decreases. Coalescence process can be divided into two categories which are the binary coalescence when the oil droplets ascend and the bulk coalescence in the dense-packed layer [28]. Smaller oil droplet size at the initial stage will lead to lower bulk coalescing rate. Hence when the oil-saline liquid system is agitated with higher rotational speed, smaller oil droplets will be generated, and the separation speed should be slower.

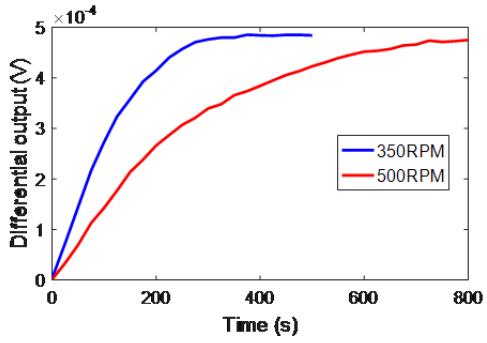

Fig. 8. Sensor outputs of two separation processes using profiles No. 2 and No. 3 in Table II.

Fig. 8 compares the simulated differential sensor outputs of two separation processes using profiles No. 2 and No. 3 in Table II. The results indicate that for the liquid with the oil fraction of 0.5, the separation time can be significantly influenced by the agitation speed and the simulation result complies with above hypothesis.

Fig. 9 illustrates the simulated sensor outputs of two separation processes using profiles No. 1 and No. 2 in Table II. The two liquid systems were both agitated with the agitation speed of 350 RPM for one hour. The inflection point of these two separation processes are similar (153.7 s and 165 s). However, by reading the differential sensor output, the separation process under the oil fraction of 0.3 seems to end earlier than that under the oil fraction of 0.5. This is because when the oil fraction is 0.3 and the lower sensing area is completely occupied with clear saline, while the separation process carries on in upper sensing area. The difference of saline volumes in the two sensing areas will remain the same and the main factor that determines the output of sensor system is the distribution of saline in the upper sensing area.

III. Experimental System

The experimental system consists of three main parts, a differential electromagnetic inductive sensor, field-programmable gate array (FPGA)-based impedance analyser, and mixing and separation system as shown in Fig. 10.

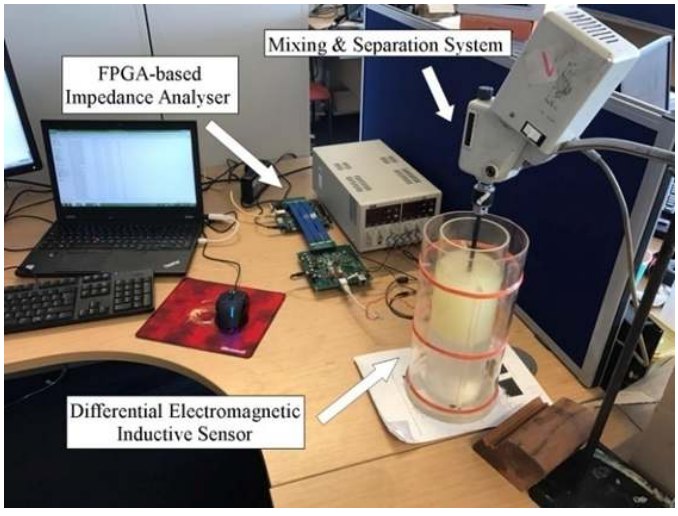

Fig. 10. Experimental System Setup.

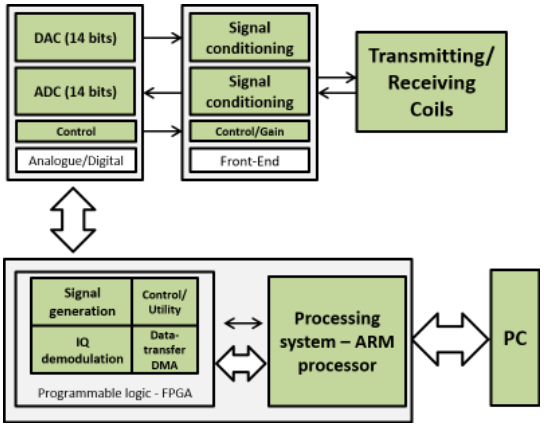

Fig. 11. System block diagram.

A. FPGA-based Impedance Analyser

A custom digital instrument is developed for measuring the impedance changes of the sensor due to magnetic induction. The instrument generates a sinusoidal signal for sensor excitation; digital signal demodulation is implemented to obtain the in-phase and quadrature components of the sensor response. The Zynq-7020 system on a chip (SoC) is the backbone of the system; this chip integrates a Xilinx 7-series FPGA and an ARM dual Cortex-A9 based processor. The instrument exploits the chip capabilities by implementing the signal generation and I/Q demodulation modules using the hardware benefits of the FPGA. The ARM processor is used for data transferring between the FPGA and a host computer.

The block diagram of the system is shown in Fig. 11. The main elements of the system include an FPGA for signal generation and I/Q demodulation, analogue-to-digital (ADC) and digital-to-analogue (DAC) converters, a front-end circuitry, and a host PC for data log, display and control.

The main elements of the Analogue/Digital block of Fig. 8 are the DAC and ADC circuits. DAC AD9767 from analog devices is used; it has two 14-bit outputs and up to 125 MSPS update rate. DAC outputs are followed by a differential-current to differential-voltage conversion and low-pass filtering stage. ADC AD6645 from analog devices is used; it has 14-bit resolution and a maximum sampling rate of 105 MSPS. The parallel digital output of the ADC is directly interfaced with the Zynq-7020 FPGA. The ADC input stage includes differential voltage translation; input swing range is ±0.55 V centred at 2.4 V. The front-end circuitry conditions and amplifies the excitation and measured signals. The output of instrument at the last amplification stage is composed of a differential pair of power amplifiers. Output voltage amplitude is 16 Vrms and fed to the excitation coil. The detection circuitry includes a RF transformer followed by several differential receivers to amplify the measured signal and feed it to the ADC. Input voltage amplitude is in millivolt range ~4 mV. Up to four measurement channels can be multiplexed and the signal gain is programmable thought the host PC. A similar architecture was presented in [19] for conductive flow measurements. For all experiments presented, excitation frequency is set to 1 MHz. The sampling frequency is 100 MHz. Data rate output is 25,000 samples per second (I/Q data). Samples are sent to a PC through an Ethernet link.

The custom instrument architecture gives two main advantages from the author perspective.

1) The hardware front-end can be customised according to the sensor/sample needs and experimental setup. A power amplifier is integrated for sensor excitation (16 Vrms as stated in manuscript). A millivolt range (~4 mV) input is expected. Integrating active amplification stages to commercial instruments commonly degrades instrument performance.
2) High data-rate output at high SNR for observing processes with different dynamics. An FPGA is used as the core of the instrument for digital signal synthesis and demodulation. FPGA can implement digital demodulation at high speed rates (100 MHz). This gives the possibility to capture the dynamics of the process with great detail during all the stages. Commonly, there is a compromise between the sample rate and the SNR, a good balance between these two figures is achieved with the custom instrument.

B. Mixing and Separation System

The mixing and separation system consists of two parts, a stirrer and a plastic baffled vessel. The stirrer (RZR 1, Heidolph UK) could achieve a maximum rotational speed of 1700 RPM. The original rod and impeller attached to the stirrer are metallic, which will interfere with inductance measurements. Hence, they were replaced with a hardwood rod coated with thermal plastic and a 3-D printed plastic impeller respectively as shown in Fig. 12. The diameter of impeller was 40 mm and the length of rod was 300 mm. These dimensions were chosen to make sure that the distance between the stirrer and coils was big enough to minimise any possible interference. The vessel was cylindrical with a diameter of 100 mm. Four full-length baffles were installed evenly on the inner vessel wall to avoid air entrapment and surface fluctuation during the mixing process.

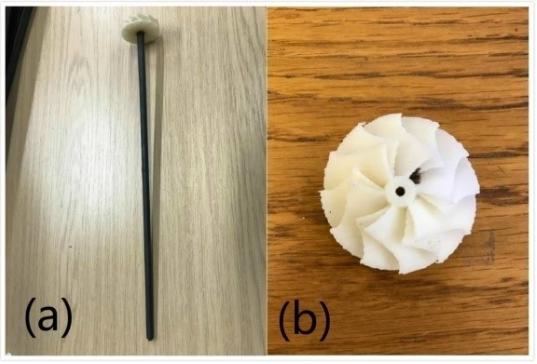

Fig. 12. (a) Hardwood rod coated with black thermal plastic tube; (b) 3-D printed plastic impeller.

IV. Experiment and Discussion

Experiments with the proposed sensor and mixing-separation system were implemented. Firstly, the validation

This article has been accepted for publication in a future issue of this journal, but has not been fully edited. Content may change prior to final publication. Citation information: DOI 10.1109/JSEN.2018.2864786, IEEE Sensors Journal

of the FPGA-based impedance analyser was carried out and the sensitivity distribution in the designed sensor system was investigate. Then the comparison between sensor output signal and saline interface height change recorded by camera was implemented to validate the sensor output. At last, the comparison on the differences of sensor outputs with respect to the change of mixing conditions such as agitation speed, mixing duration and oil fraction was implemented. Based upon these validations and comparisons, the sensor's capability of identifying the completion level and separation speed under different circumstances can be investigated.

The separation process of oil and saline highly relies on the oil droplet size distribution. The oil droplet size distribution is determined by the agitation speed and mixing duration. With higher agitation speed and longer mixing duration, the separation speed is expected to be slower.

A. Validation of Instrument

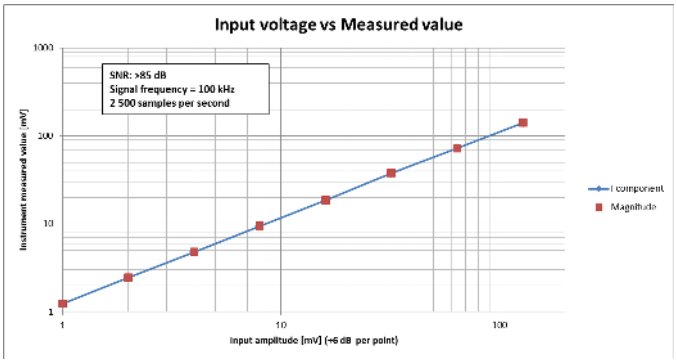

Fig. 13. The instrument performance for measuring a voltage signal.

The validation of the instrument was carried out. Fig. 13 shows the instrument performance for measuring a voltage signal. The figure shows the nominal value of the input signal in the 'x' axis; voltage range is in millivolt range. Instrument measured values for the magnitude and imaginary component are plotted in the 'y' axis. A proportional increase in the measurement can be observed for the corresponding increase in the input signal. For this experiment an SNR greater than 85 dB is achieved for all measurement points.

B. Validation of Sensitivity Distribution

Experimental tests were carried out to evaluate the actual sensitivity distribution by continuously adding saline saline into the separation vessel. The corresponding output signal is shown in Fig. 14. When the planar sensitivity distribution is uniform, the sensor outputs tend to increase proportionally before the interface of saline reaches the transmitting coil plane and drop proportionally after the interface exceeds the plane. The Λ-shaped curve in Fig. 14 implies that the vertical sensitivity distribution is uniform enough for the experiment.

C. Validation of Sensor Output

A camera was set up to record the behaviour of the oil-saline mixture during the separation process and the sensor

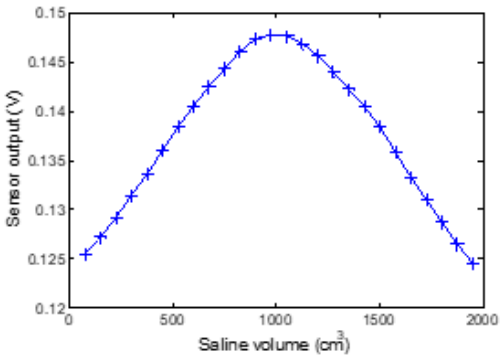

Fig. 14. Experimental test result for sensitivity distribution with saline saline.

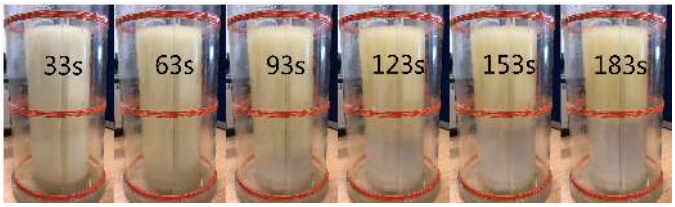

Fig. 15. Screenshots from the recorded video during the separation process.

output was also recorded synchronously. The oil fraction was 50% in this experiment and the initial height of the interface between oil and saline was 125 mm. Firstly, the liquid system was agitated for 30 seconds under the agitation speed of 1700 RPM. Then the agitation was stopped to allow the mixture separation for 270 seconds. Some screenshots from the recorded video during the separation process are shown in Fig. 15. A clear interface between saline and the contents above (oil and oil-saline mixture) can be observed in the video. The height change of the interface was measured at corresponding time and the results are compared with the sensor output in Fig. 16.

The interface height indicates the completion level of the separation process. From the comparison in Fig. 16, it is clear that the overall trend of sensor signal change complied with the interface height change. The signal started to increase when separation began and became steady when the separation process was approaching the end. However, differences exist between the two curves. This could be explained with the

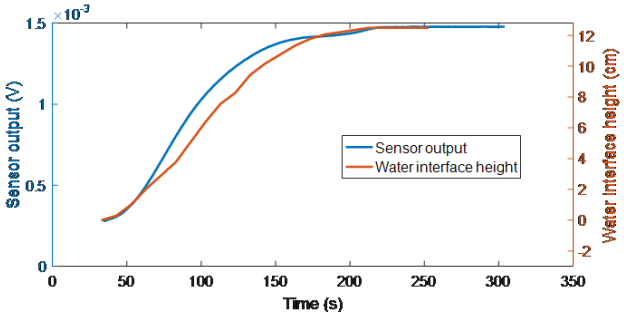

Fig. 16. Comparison between sensor output and saline interface height change during the separation process.

This article has been accepted for publication in a future issue of this journal, but has not been fully edited. Content may change prior to final publication. Citation information: DOI 10.1109/JSEN.2018.2864786, IEEE Sensors Journal

structure of oil-saline separation system discussed in Section II. The liquid above the clear saline volume includes oil and oil-saline mixture. The sensor output reflects the distribution of both the clear saline in the bottom volume and the saline component in oil-saline mixture in the top volume, while the saline interface height captured by camera only indicates the volume of saline in the vessel. Hence, the difference of the two curves is caused by the saline component in oil-saline mixture.

In conclusion, the comparison made between the sensor output signal and saline interface height during the same separation process indicates that the proposed instrument is capable of detecting the final separation stage of the process. This serves as an initial validation of the application of DEMIS in monitoring oil-saline separation. Further validation which involves on-site facilities would be useful and we leave it for further studies.

D. Experiment results under different mixing conditions

1) 1700 RPM Agitation Speed and 50% Oil Fraction: Fig. 17 shows the variations of the sensor output as a function of time when the agitation speed and oil fraction were fixed as 1700 RPM and 50% respectively. Tests with three different mixing durations, namely, 30 seconds, 5 minutes and 15 minutes were investigated. Each experiment was repeated for three times and the corresponding sensor outputs were recorded. It can be seen from Fig. 17 that the results in each experiment are highly repeatable and consistent.

In Fig. 18, the averaged sensor outputs of the three repeat experiments during the separation stage for the three different mixing durations are compared. The standard deviation on each time point is also calculated and presented on the curves as error bars. The starting points of the three curves are rather close to each other, which indicates that the liquid systems were all fully mixed and the volume distributions of oil were similar in all three groups when the separation started. However, the difference in separation speeds under different mixing durations can be observed clearly. This can be attributed to the different oil droplet sizes. The longer the mixing duration, the smaller the average droplet size, and the slower the separation speed. After the separation completed, the sensor output value of the three groups stayed approximately at the same level as the one before mixing started. This shows that the oil and saline recovered to the state where they were completely separated.

2) 900 RPM Agitation Speed and 50% Oil Fraction: The experiment results when the agitation speed was 900 RPM are shown in Fig. 19. In this case, at the beginning of the separation process, the average initial sensor output values of the three groups were different. The initial value was larger when the mixing duration was shorter. This is mainly because the liquid system was not fully mixed and there was an oil layer remaining at the top of the mixing vessel, resulting in a higher differential output from the sensors when the separation started. In addition, the standard deviations of the repeat tests were also getting larger comparing to those of the 1700 RPM agitation speed. When the liquid system was not

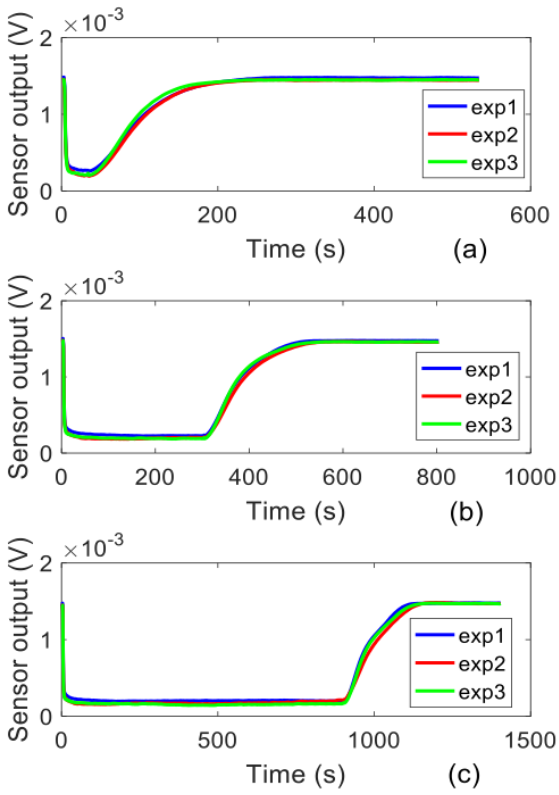

Fig. 17. Sensor outputs of repeat experiments under agitation speed of 1700 RPM, oil fraction 50%. (a) mixing duration 30 seconds; (b) mixing duration 5 minutes; (c) mixing duration 15 minutes.

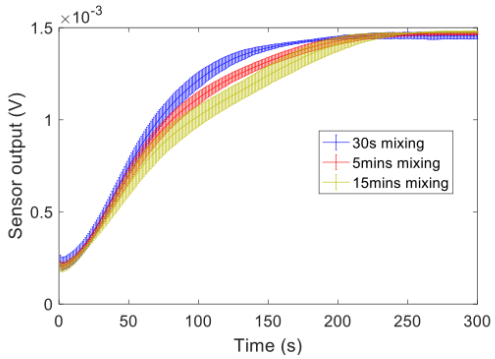

Fig. 18. Average sensor outputs of the repeat test under 1700 RPM during separation process.

fully mixed, the oil droplet size distribution would become much more spread out, which led to large variations of the differential sensor output. It should be noted that the overall separation speed was still slower when the mixing duration became longer, as the resulted average oil droplet size was correspondingly smaller.

3) 1700 RPM Agitation Speed and 33% Oil Fraction: Fig. 20 presents the results with the agitation speed of 1700 RPM but a lower oil fraction of 33%. It can be seen that the results are also highly consistent with the simulation results. The difference in separation speed among the three groups is

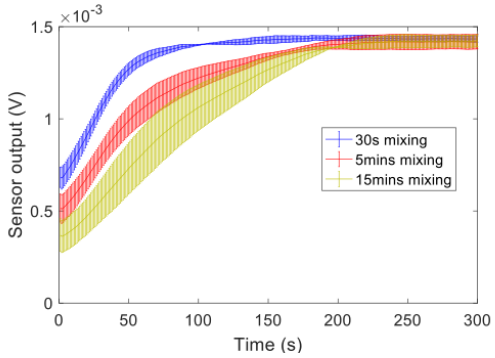

Fig. 19. Average sensor outputs of the repeat test under 900 RPM during separation process.

as a result of different mixing duration, which leads to different average oil droplet sizes. The curves of separation process enter stable stage earlier than those with the oil fraction of 50%. The reason has already been explained in the simulation section as when the lower testing area is filled with clear saline, the change of sensor output will depend on the saline phase distribution in the top sensing region.

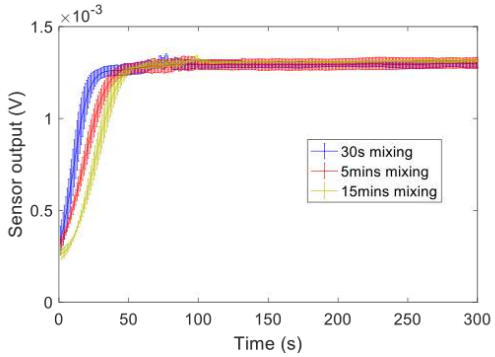

Fig. 20. Average sensor outputs of the repeat test at oil fraction of 33% under 1700 RPM during separation process.

V. Conclusions

The paper investigated the use of a proposed three-coil differential electromagnetic inductive sensing system for monitoring the oil and saline separation process. The sensor was optimised using electromagnetic computation models to achieve uniform vertical sensitivity. A theoretical liquid-liquid batch settling models was applied for describing the separation processes. Experiments under different oil-saline fractions (33% and 50%), different agitation speeds (900 RPM and 1700 RPM) and durations (0.5 minutes, 5 minutes and 15 minutes) have been conducted. The error of the sensor outputs for repeated experiments was within 16%. The results indicate that the proposed sensor system is able to measure the separation process of oil and saline under different circumstances. Considering the practical oil-saline separation as a continuous process, the measurement information could be interpreted into the interface location information in the separation vessel and saline and oil outlet speed can be adjusted accordingly to guarantee product quality. In conclusion, the non-intrusive and non-invasive nature of the electromagnetic inductive sensing technique suggests it is a promising method for in-situ monitoring of oil-saline separations in industrial applications.

References

[1] J. Behin and M. Aghajari, "Influence of water level on oil–water separation by residence time distribution curves investigations," *Separation and Purification Technology*, vol. 64, pp. 48–55, Nov. 2008.
[2] G. Fowles, *Flow, Level and Pressure Measurement in the Water Industry - 1st Edition*. Butterworth-Heinemann, Jan. 1994.
[3] N. Dave, "Magnetostrictive linear position sensors," *Sensors-the Journal of Applied Sensing Technology*, vol. 16, no. 11, pp. 38–47, 1999.
[4] M. Pasquale, "Mechanical sensors and actuators," *Sensors and Actuators A: Physical*, vol. 106, pp. 142–148, Sept. 2003.
[5] A. J. Jaworski and G. Meng, "On-line measurement of separation dynamics in primary gas/oil/water separators: Challenges and technical solutions—A review," *Journal of Petroleum Science and Engineering*, vol. 68, pp. 47–59, Sept. 2009.
[6] S. F. A. Bukhari and W. Yang, "Multi-interface Level Sensors and New Development in Monitoring and Control of Oil Separators," *Sensors*, vol. 6, pp. 380–389, Apr. 2006.
[7] B. T. Hjertaker, G. A. Johansen, and P. Jackson, "Recent developments in hydrocarbon separator interface imaging," in *Process Imaging for Automatic Control*, vol. 4188, pp. 81–93, International Society for Optics and Photonics, Feb. 2001.
[8] W. Yang, "Sensors and Instrumentation for Monitoring and Control of Multi-Phase Separation," *Measurement and Control*, vol. 39, pp. 178–184, July 2006.
[9] M. S. A. Abouelwafa and E. J. M. Kendall, "The measurement of component ratios in multiphase systems using alpha -ray attenuation," *Journal of Physics E: Scientific Instruments*, vol. 13, no. 3, p. 341, 1980.
[10] W. A. S. Kumara, B. M. Halvorsen, and M. C. Melaaen, "Single-beam gamma densitometry measurements of oil–water flow in horizontal and slightly inclined pipes," *International Journal of Multiphase Flow*, vol. 36, pp. 467–480, June 2010.
[11] M. Meribout, A. A. Naamany, and K. A. Busaidi, "Interface Layers Detection in Oil Field Tanks: A Critical Review," p. 30.
[12] N.-O. Skeie and M. Halstensen, "Level estimation in oil/water separators based on multiple pressure sensors and multivariate calibration," *Journal of Chemometrics*, vol. 24, pp. 387–398, July 2010.
[13] B. K. Arvoh, N.-O. Skeie, and M. Halstensen, "Estimation of gas/liquid and oil/water interface levels in an oil/water/gas separator based on pressure measurements and regression modelling," *Separation and Purification Technology*, vol. 107, pp. 204–210, Apr. 2013.
[14] A. J. Jaworski and T. Dyakowski, "Measurements of oil–water separation dynamics in primary separation systems using distributed capacitance sensors," *Flow Measurement and Instrumentation*, vol. 16, pp. 113–127, Apr. 2005.
[15] O. Isaksen, A. S. Dico, and E. A. Hammer, "A capacitance-based tomography system for interface measurement in separation vessels," *Measurement Science and Technology*, vol. 5, no. 10, p. 1262, 1994.
[16] W. Q. Yang, "Further developments in an ac-based capacitance tomography system," *Review of Scientific Instruments*, vol. 72, pp. 3902–3907, Sept. 2001.
[17] A. Shafquet, I. Ismail, A. Japper-Jaafar, S. A. Sulaiman, and G. T. Chala, "Estimation of gas void formation in statically cooled waxy crude oil using online capacitance measurement," *International Journal of Multiphase Flow*, vol. 75, pp. 257–266, Oct. 2015.
[18] W. Yin, A. J. Peyton, G. Zysko, and R. Denno, "Simultaneous Noncontact Measurement of Water Level and Conductivity," *IEEE Transactions on Instrumentation and Measurement*, vol. 57, pp. 2665–2669, Nov. 2008.
[19] T. Yang, G. Chen, W. Yin, P. Hu, and Q. Zhao, "A high frequency digital induction system for condutive flow level measurements," *Flow Measurement and Instrumentation*, vol. 37, pp. 83–91, June 2014.
[20] K. Asskildt and P. Hansson, "New measuring sensor for level detection in subsea separators," *ABB Review*, pp. 11–17, Apr. 1994.
[21] D. N. Dyck, D. A. Lowther, and E. M. Freeman, "A method of computing the sensitivity of electromagnetic quantities to changes in materials and sources," *IEEE Transactions on Magnetics*, vol. 30, pp. 3415–3418, Sept. 1994.
[22] W. Yin and A. J. Peyton, "Sensitivity Formulation Including Velocity Effects for Electromagnetic Induction Systems," *IEEE Transactions on Magnetics*, vol. 46, pp. 1172–1176, May 2010.

[23] S. A. K. Jeelani and S. Hartland, "Effect of Dispersion Properties on the Separation of Batch Liquid-Liquid Dispersions," *Industrial & Engineering Chemistry Research*, vol. 37, pp. 547–554, Feb. 1998.
[24] S. Al-Zuhair, "Using liquid–liquid deep settling model in determining the design parameters of crude palm oil settler," *Separation and Purification Technology*, vol. 35, pp. 133–140, Feb. 2004.
[25] G.-Z. Yu and Z.-S. Mao, "Sedimentation and Coalescence Profiles in Liquid-Liquid Batch Settling Experiments," *Chemical Engineering & Technology*, vol. 27, no. 4, pp. 407–413.
[26] Y. Faraj, M. Wang, J. Jia, Q. Wang, C.-g. Xie, G. Oddie, K. Primrose, and C. Qiu, "Measurement of vertical oil-in-water two-phase flow using dual-modality ERT–EMF system," *Flow Measurement and Instrumentation*, vol. 46, pp. 255–261, Dec. 2015.
[27] G. K. Batchelor, *An Introduction to Fluid Dynamics*. Cambridge University Press, Feb. 2000. Google-Books-ID: Rla7OihRvUgC.
[28] S. a. K. Jeelani and S. Hartland, "Prediction of steady state dispersion height from batch settling data," *AIChE Journal*, vol. 31, no. 5, pp. 711–720.

Shupei Wang received the B.Eng. in Microelectronics from East China Normal University, Shanghai, China in 2011, and the M.Sc. in Electrical Power from Newcastle University, Newcastle Upon Tyne, U.K. in 2013. He is currently pursuing the Ph.D. degree in Electrical and Electronic Engineering with the University of Manchester, Manchester, U.K. His research interests include industrial process monitoring, electromagnetic sensors, electromagnetic simulations, electrical resistance tomography, inverse problem algorithms, non-destructive testing and etc.

Ruozhou Hou has over 20 years of research experiences in multidisciplinary fields including chemical engineering, particle technology, process engineering and monitoring, sensing and instrumentation, transducer design, characterisation and simulation. He joined the School of Chemical Engineering and Analytical Science, University of Manchester in 2013, and has been working as a postdoc research associate/experimental officer on mixing power characterisation, concentrated viscous or viscoelastic aqueous suspension productions, and use of electrical resistance tomography for process monitoring and analysis.

Jorge Ricardo Salas Avila received the B.S. in Electronic and Computer Engineering from the Monterrey Institute of Technology and Higher Education, Chihuahua, Mexico in 2010, and the M. Sc. in Informatics Technology from the Monterrey Institute of Technology and Higher Education, Monterrey, Mexico in 2013. He is currently pursuing the Ph.D. degree in electrical and electronic engineering with the University of Manchester, Manchester, U.K. His current research interests include instrumentation, electromagnetic sensors, FPGA-based digital instruments and non-destructive testing.

Yang Tao received a B.Sc. in Automation from Tianjin University, Tianjin, China, in 2010, a M.Sc. in Control Science and Engineering also from Tianjin University in 2013 and the PhD in Electrical and Electronic Engineering in The University of Manchester, Manchester, U.K. in 2018. He is currently working as an research associate in the school of electrical and electronic engineering, The University of Manchester.

His research interests include electromagnetic instrumentation, metal detection, multi-frequency power inverter, electromagnetic tomography, inverse problem, sparse representation and deep learning.

Wuliang Yin (M'05–SM'06) was appointed as an MT Sponsored Lecturer with the School of Electrical and Electronic Engineering, University of Manchester, Manchester, U.K., in 2012, and was promoted to Senior Lecturer in 2016. He has authored one book, more than 180 papers, and was granted more than ten patents in the area of electromagnetic (EM) sensing and imaging.

Dr. Yin was a recipient of the 2014 and 2015 Williams Award from the Institute of Materials, Minerals and Mining and the Science and Technology Award from the Chinese Ministry of Education in 2000.